Anal. Chem. **2006,** *78,* 3452−3460

Carbon-13 Labeled Polymers: An Alternative Tracer for Depth Profiling of Polymer Films and Multilayers Using Secondary Ion Mass Spectrometry

S. E. Harton,[†] F. A. Stevie,[‡] Z. Zhu,[‡] and H. Ade*[,§]

Department of Materials Science & Engineering, Analytical Instrumentation Facility, and Department of Physics, North Carolina State University, Raleigh, North Carolina 27695

^{13}C labeling is introduced as a tracer for depth profiling of polymer films and multilayers using secondary ion mass spectrometry (SIMS). Deuterium substitution has traditionally been used in depth profiling of polymers but can affect the phase behavior of the polymer constituents with reported changes in both bulk-phase behavior and surface and interfacial interactions. SIMS can provide contrast by examining various functional groups, chemical moieties, or isotopic labels. ^{13}C-Labeled PS (^{13}C-PS) and unlabeled PS (^{12}C-PS) and PMMA were synthesized using atom-transfer radical polymerization and assembled in several model thin-film systems. Depth profiles were recorded using a Cameca IMS-6f magnetic sector mass spectrometer using both 6.0-keV impact energy Cs^+ and 5.5-keV impact energy O_2^+ primary ion bombardment with detection of negative and positive secondary ions, respectively. Although complete separation of $^{12}C^1H$ from ^{13}C is achieved using both primary ion species, 6.0-keV Cs^+ clearly shows improved detection sensitivity and signal-to-noise ratio for detection of ^{12}C, $^{12}C^1H$, and ^{13}C secondary ions. The use of Cs^+ primary ion bombardment results in somewhat anomalous, nonmonotonic changes in the ^{12}C, $^{12}C^1H$, and ^{13}C secondary ion yields through the PS/PMMA interface; however, it is shown that this behavior is not due to sample charging. Through normalization of the ^{13}C secondary ion yield to the total C ($^{12}C + {}^{13}C$) ion yield, the observed effects through the PS/PMMA interface can be greatly minimized, thereby significantly improving analysis of polymer films and multilayers using SIMS. Mass spectra of ^{13}C-PS and ^{12}C-PS were also analyzed using a PHI TRIFT I time-of-flight mass spectrometer, with 15-keV Ga^+ primary ion bombardment and detection of positive secondary ions. The $^{12}C_7{}^1H_7$ ion fragment and its ^{13}C-enriched analogues have significant secondary ion yields with negligible mass interferences, providing an early indication of the potential for future use of this technique for cluster probe depth profiling of high molecular weight ^{13}C-labeled fragments.

Advances in one-dimensional depth profiling of polymer films have provided a significant driving force for growth in experimental and theoretical polymer physics over the past 20 years.[1] Particularly useful for investigations involving thin films (<1 μm), these measurements generally focus on probing various physical phenomena related to two-dimensional confinement of polymer chains, including segregation phenomena[2] and diffusion properties near surfaces and heterogeneous interfaces.[3] Several experimental techniques have been used for depth profiling of polymer films and multilayers,[1] including neutron (NR), X-ray, or resonant X-ray reflectometry,[4,5] Rutherford backscattering,[6] forward recoil spectrometry (FRES),[7] nuclear reaction analysis (NRA),[8] and secondary ion mass spectrometry (SIMS).[9,10] These techniques are frequently used to probe the concentration of a labeled polymer, often deuterium (^2H) substituted,[1] as a function of depth to observe various phenomena, including reactive coupling at polymer interfaces,[11,12] polymer chain mobility near surfaces and interfaces,[13,14] surface or interfacial segregation,[15,16] and block copoly-

* Corresponding author. E-mail: harald_ade@ncsu.edu.
† Department of Materials Science & Engineering.
‡ Analytical Instrumentation Facility.
§ Department of Physics.

(1) Kramer, E. J. *Physica B* **1991**, *173*, 189.
(2) Jones, R. A. L.; Kramer, E. J.; Rafailovich, M. H.; Sokolov, J.; Schwarz, S. A. *Phys. Rev. Lett.* **1989**, *62*, 280.
(3) Zheng, X.; Rafailovich, M. H.; Sokolov, J.; Y, S.; Schwarz, S. A.; Sauer, B. B.; Rubinstein, M. *Phys. Rev. Lett.* **1997**, *79*, 241.
(4) Roe, R.-J. *Methods of X-ray and Neutron Scattering in Polymer Science*; Oxford University Press: New York, 2000.
(5) Wang, C.; Araki, T.; Ade, H. *Appl. Phys. Lett.* **2005**, *87*, 214109.
(6) Composto, R. J.; Kramer, E. J. *J. Mater. Sci.* **1991**, *26*, 2815.
(7) Composto, R. J.; Walters, R. M.; Genzer, J. *Mater. Sci. Eng., R* **2002**, *38*, 107.
(8) Chaturvedi, U. K.; Steiner, U.; Zak, O.; Krausch, G.; Schatz, G.; Klein, J. *Appl. Phys. Lett.* **1990**, *56*, 1228.
(9) Schwarz, S. A.; Wilkens, B. J.; Pudensi, M. A. A.; Rafailovich, M. H.; Sokolov, J.; Zhao, X.; Zhao, W.; Zheng, X.; Russell, T. P.; Jones, R. A. L. *Mol. Phys.* **1992**, *76*, 937.
(10) Harton, S. E.; Stevie, F. A.; Ade, H. *J. Vac. Sci. Technol., A* **2006**, *24*, 362.
(11) Kim, B. J.; Kang, H.; Char, K.; Katsov, K.; Fredrickson, G. H.; Kramer, E. J. *Macromolecules* **2005**, *38*, 6106.
(12) Harton, S. E.; Stevie, F. A.; Spontak, R. J.; Koga, T.; Rafailovich, M. H.; Sokolov, J. C.; Ade, H. *Polymer* **2005**, *46*, 10173.
(13) Russell, T. P.; Deline, V. R.; Dozier, W. D.; Felcher, G. P.; Agrawal, G.; Wool, R. P.; Mays, J. W. *Nature* **1993**, *365*, 235.
(14) Zheng, X.; Sauer, B. B.; Alsten, J. G. V.; Schwarz, S. A.; Rafailovich, M. H.; Sokolov, J.; Rubinstein, M. *Phys. Rev. Lett.* **1995**, *74*, 407.
(15) Hariharan, A.; Kumar, S. K.; Rafailovich, M. H.; Sokolov, J.; Zheng, X.; Duong, D. H.; Schwarz, S. A.; Russell, T. P. *J. Chem. Phys.* **1993**, *99*, 656.
(16) Reynolds, B. J.; Ruegg, M. L.; Mates, T. E.; Radke, C. J.; Balsara, N. P. *Macromolecules* **2005**, *38*, 3872.

10.1021/ac060133o CCC: $33.50
Published on Web 04/08/2006

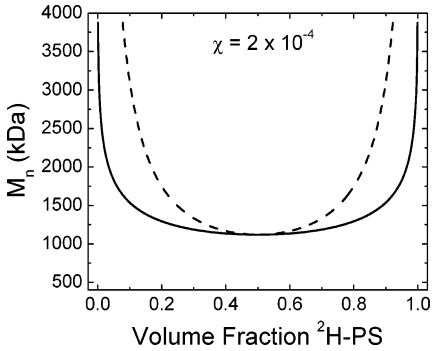

Figure 1. Isothermal phase diagram of a symmetric blend (both polymers have the same number of monomeric segments) of 100% deuterium substituted PS (^{2}H-PS) and unlabeled PS (^{1}H-PS) generated using parameters from ref. 20, assuming a concentration-independent (nominal) mean-field interaction parameter $\chi = 2 \times 10^{-4}$ (~125 °C). The solid line is the binodal (coexistence curve), while the dashed line is the spinodal. At high molecular weights (^{2}H-PS M_n > 1120 kDa) classical phase separation, such as nucleation and growth and spinodal decomposition, can occur.

mer ordering.[17,18] Even though deuterium substitution has led to many advances, it can affect the phase behavior of the polymer constituents with reported changes in both bulk phase behavior (see Figure 1)[19,20] and surface and interfacial interactions.[2,15] More recently, it was found that deuterium substitution can have a profound effect on the properties of a polymer/polymer heterogeneous interface, with the observation of diffusion-controlled segregation of deuterium-labeled polystyrene (^{2}H-PS) to a ^{1}H-PS:^{2}H-PS/poly(methyl methacrylate) (PMMA) interface.[21] Because deuterium labeling can introduce changes in the properties being measured, alternative methods of tracer labeling are desired for optimal analysis. This paper details the development of one such method.

While the commonly used techniques NR, FRES, and NRA rely on deuterium substitution to provide contrast in polymer films, SIMS can utilize the contrast provided by various functional groups, chemical moieties, or isotopic labels.[9,22,23] This makes SIMS particularly versatile for depth profiling of polymer films and multilayers, although this versatility comes at a cost. Depth profiling using SIMS is particularly sensitive to matrix effects induced by changing densities or chemical environments,[24,25] which are encountered at polymer surfaces, polymer/polymer heterogeneous interfaces, and polymer/inorganic substrate interfaces. SIMS involves bombarding a target film with primary ions, such as O_2^+, O^-, Cs^+, Ar^+, Xe^+, Au^+, Ga^+, and C_{60}^+, and detecting positive or negative secondary ions that are sputtered from the surface.[23,26,27] When the primary ion fluence is below the so-called static limit (~10^{12}–10^{13} ions/cm^2),[28] detection is primarily from the top monolayer (~1 nm) of the film. This is the static SIMS technique, which is useful for observing surface composition or two-dimensional surface imaging.[27] For one-dimensional depth profiling (dynamic SIMS), or even three-dimensional imaging,[29] analysis conditions must be implemented where the primary ion fluence is above the static limit, thereby causing an erosion of the film at a controlled rate (sputtering rate S_R). This allows for information to be obtained regarding chemical composition as a function of depth through the sample. With dynamic SIMS, though, the chemical information obtainable is often quite different from that with static SIMS analysis, as ion-induced mixing and chemical degradation can significantly alter the chemical structures below the surface.[27,30] This often limits profiling of organic species to simple atomic or diatomic species, such as H, C, CH, O, CN, and Br.[9]

SIMS instruments have three types of mass analyzers, namely, quadrupole, magnetic sector, and time-of-flight (TOF).[31] Quadrupole mass spectrometers are commonly used for depth profiling of various types of samples, including metals, semiconductors, and organics. Because of the low primary ion impact energies possible with these instruments (<1 keV), subnanometer depth resolutions are possible when depth profiling highly structured semiconductors,[31] and depth resolutions less than 10 nm have been reported for depth profiling of polymer films and multilayers.[15,16] These instruments are limited by low mass resolution (typical $m/\Delta m \sim 300$),[31] making it impossible to completely separate (mass resolve) secondary ions with identical nominal masses, such as ^{2}H (2.014 amu) from $^1H_2$ (2.015 65 amu) and ^{13}C (13.00 335 amu) from $^{12}C^1H$ (13.007 82 amu).[23] Quadrupole instruments can, however, be used for depth profiling of deuterium-labeled polymers, as there is negligible mass interference from $^1H_2^-$ when detecting negative ions.[9] In contrast to quadrupole instruments, magnetic sector mass spectrometers have relatively high mass resolving capabilities, with a maximum $m/\Delta m \sim 2 \times 10^4$, although $(6-8) \times 10^3$ is somewhat of a practical upper limit for maintaining reasonable detection sensitivity.[31] These instruments can mass resolve secondary ion species such as ^{2}H from $^1H_2$ and ^{13}C from $^{12}C^1H$ with detection of positive or negative secondary ions.[10,23] Transmission of secondary ions into the detector is much greater for magnetic sector instruments than with quadrupole instruments,[31] but charging is often problematic for the analysis of insulators.[32] These problems can be overcome with various active or passive charge neutralization measures that include a conductive coating, negative primary ions (e.g., O^-), and electron bombardment.[32,33] Time-of-flight mass spectrometers

(17) Coulon, G.; Russell, T. P.; Deline, V. R.; Green, P. F. *Macromolecules* **1989**, *22*, 2581.
(18) Anastasiadis, S. H.; Russell, T. P.; Satija, S. K.; Majkrzak, C. F. *J. Chem. Phys.* **1990**, *92*, 5677.
(19) Russell, T. P. *Macromolecules* **1993**, *26*, 5819.
(20) Budkowski, A.; Steiner, U.; Klein, J.; Schatz, G. *Europhys. Lett.* **1992**, *18*, 705.
(21) Harton, S. E.; Stevie, F. A.; Ade, H. *Macromolecules* **2006**, *39*, 1639.
(22) Harrison, C.; Park, M.; Chaikin, P. M.; Register, R. A.; Adamson, D. H.; Yao, N. *Polymer* **1998**, *39*, 2733.
(23) Wilson, R. G.; Stevie, F. A.; Magee, C. W. *Secondary Ion Mass Spectrometry: A Practical Handbook for Depth Profiling and Bulk Impurity Analysis*; John Wiley & Sons: New York, 1989.
(24) Deline, V. R.; Katz, W.; Evans, C. A.; Williams, P. *Appl. Phys. Lett.* **1978**, *33*, 832.
(25) Wilson, R. G.; Lux, G. E.; Kirschbaum, C. L. *J. Appl. Phys.* **1993**, *73*, 2524.
(26) Honig, R. E. *J. Appl. Phys.* **1958**, *29*, 549.
(27) Winograd, N. *Anal. Chem.* **2005**, *77*, 142A.
(28) Honig, R. E. *Int. J. Mass Spectrom. Ion Processes* **1985**, *66*, 31.
(29) Jerome, J.; Zhu, S.; Seo, Y. S.; Ho, M.; Pernodet, N.; Gambino, R.; Sokolov, J.; Rafailovich, M. H.; Zaitsev, V.; Schwarz, S.; DiNardo, R. *Macromolecules* **2004**, *37*, 6504.
(30) Postawa, Z.; Czerwinski, B.; Winograd, N.; Garrison, B. J. *J. Phys. Chem. B* **2005**, *109*, 11973.
(31) Chia, V. K. F.; Mount, G. R.; Edgell, M. J.; Magee, C. W. *J. Vac. Sci. Technol., B* **1999**, *17*, 2345.
(32) Pivovarov, A. L.; Stevie, F. A.; Griffis, D. P. *Appl. Surf. Sci.* **2004**, *231–232*, 786.
(33) Migeon, H. N.; Schuhmacher, M.; Slodzian, G. *Surf. Interface Anal.* **1990**, *16*, 9.

have seen significant growth in recent years, particularly with developments of the so-called cluster probes (e.g., Au_3^+, SF_5^+, and C_{60}^+).[27,34] Their mass range, mass resolution, and secondary ion transmission generally exceed that for the other analyzers. Although their use has been restricted primarily to static SIMS (compositional analysis and two-dimensional imaging),[35] TOF SIMS have seen some use in depth profiling of tracer-labeled polymers in polymer films,[36] and their use in depth profiling of somewhat high molecular weight species or fragments (~100 amu) has received considerable attention in recent years.[37−40]

Here, we demonstrate and detail the use of ^{13}C labeling for depth profiling of polymer films and multilayers. PS was synthesized with ^{13}C-labeled styrene monomer (^{13}C-PS) and analyzed in multilayers containing films of ^{13}C-PS or ^{13}C-PS/unlabeled PS (^{12}C-PS) blends. Using a Cameca IMS-6f magnetic sector mass spectrometer, we were able to mass resolve $^{12}C^1H$ from ^{13}C with $m/\Delta m \approx 3000$. Two primary ions were investigated, O_2^+ and Cs^+, with detection of positive and negative secondary ions, respectively.[10] O_2^+ and Cs^+ are two commercially available primary ion sources that are commonly used for depth profiling using SIMS.[23,24,31,41,42] Their use is well known to provide enhanced secondary ion yields when compared to primary ion bombardment using inert gases, such as Ar^+.[43−46] It was found that Cs^+ provides considerably higher ^{12}C, ^{13}C, and $^{12}C^1H$ detection sensitivity than O_2^+ for the conditions implemented, but the interface between PS and PMMA is more susceptible to matrix effects with Cs^+ primary ion bombardment. Because a submatrix (^{13}C) is analyzed and can be normalized to the total carbon secondary ion yield ($^{12}C + {}^{13}C$) to convert the secondary ion yield to ^{13}C-PS concentration, a reduction in matrix effects encountered at the PS/PMMA interface can be realized. Mass spectra of ^{13}C-PS and ^{12}C-PS were measured using a PHI TRIFT I TOF mass spectrometer (static SIMS) with Ga^+ primary ion bombardment and detection of positive secondary ions. These results demonstrate the potential for future use of TOF SIMS for depth profiling high molecular weight (~100 amu) fragments of ^{13}C-labeled polymers. ^{13}C labeling of polymers should thus be a very beneficial approach for analysis using TOF or magnetic sector SIMS, and the ^{13}C-labeling method presented here should be applicable for analysis of various soft condensed matter systems in fields ranging from polymer science to biology.

EXPERIMENTAL SECTION

Polymer Synthesis. ^{13}C-PS, ^{12}C-PS, and PMMA were synthesized using atom-transfer radical polymerization.[47] The chemical structures of PS and PMMA are shown in Figure 2. The

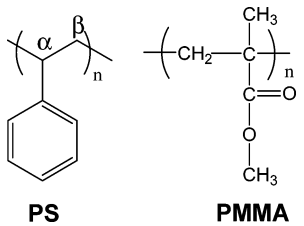

PS PMMA

Figure 2. Chemical structures for PS and PMMA. α and β are the backbone carbons in PS, both of which are ^{13}C substituted in the ^{13}C-labeled styrene monomer.

polymerization mechanisms and procedures have been described in detail previously[48] and will only be briefly outlined here. Before the synthesis was performed, copper(I) bromide (98% CuBr, Sigma-Aldrich) was purified according to established procedures.[49] Initiator, ligand, and solvent were used as received. For synthesis of atactic ^{13}C-PS, 2 mL of unlabeled styrene (99%, Sigma-Aldrich) and 1 mL of α,β-^{13}C-labeled styrene monomer (99%, Isotec) were put through a neutral activated alumina column. Into a 10-mL Schlenk flask, 10.5 mg of CuBr, 16 μL of *N*,*N*,*N*′,*N*′,*N*″-pentamethyldiethylenetriamine (99% PMDETA, Sigma-Aldrich), and monomer were added. The flask was sealed with a rubber septum, and the solution was bubbled with N_2 for 20 min to remove O_2. Next, 4.2 μL of 1-bromoethylbenzene (97% BrEb, Sigma-Aldrich) was injected into the solution, the flask was immersed in an oil bath held at 110 °C, and its contents were continuously stirred using a magnetic stir bar. After 7.5 h, the reaction was stopped (~75% monomer conversion), and the solution was diluted with tetrahydrofuran (THF, Acros) and run through a neutral activated alumina column to remove the CuBr. This solution was precipitated into 1 L of methanol (MeOH, Fisher), filtered, and dried overnight at 70 °C. For atactic ^{12}C-PS synthesis, 50 mL of styrene, which had been put through a neutral activated alumina column, 144 mg of CuBr, and 210 mL of PMDETA were added to a 100-mL round-bottom flask. The flask was sealed with a rubber septum, bubbled with N_2 for 25 min, and 70 μL of BrEb was injected into the solution. The solution and flask was immersed in an oil bath held at 110 °C with continuous stirring. After 6.5 h, the reaction was stopped and the solution was diluted with THF and run through a neutral activated alumina column. This solution was precipitated into 2 L of MeOH, filtered, and dried overnight at 70 °C. The molecular weights and polydispersities of ^{12}C-PS and ^{13}C-PS were measured using gel permeation chromatography (GPC) with a chloroform diluent at 30 °C, after calibration with atactic PS standards (Polymer Laboratories). Using differential scanning calorimetry (DSC), with a cooling cycle of 10 °C/min, the inflection-point glass transition temperatures (T_g's) were determined to be 100 °C for both ^{12}C-PS and ^{13}C-PS.

For synthesis of PMMA, methyl methacrylate (>99%, Fluka) was put through a basic activated alumina column. To a 125-mL round-bottom flask, 30 mL of monomer, 30 mL of phenyl ether (99%, Acros), 43 mg of CuBr, and 63 μL of PMDETA were added. The flask was sealed with a rubber septum and bubbled with N_2

(34) Weibel, D.; Wong, S.; Lockyer, N.; Blenkinsopp, P.; Hill, R.; Vickerman, J. C. *Anal. Chem.* **2003**, *75*, 1754.
(35) Castner, D. G. *Nature* **2003**, *422*, 129.
(36) Hu, X.; Zhang, W.; Si, M.; Gelfer, M.; Hsiao, B.; Rafailovich, M.; Sokolov, J.; Zaitsev, V.; Schwarz, S. *Macromolecules* **2003**, *36*, 823.
(37) Fuoco, E. R.; Gillen, G.; Wijesundara, M. B. J.; Wallace, W. E.; Hanley, L. *J. Phys. Chem. B* **2001**, *105*, 3950.
(38) Wagner, M. S. *Anal. Chem.* **2005**, *77*, 911.
(39) Szakal, C.; Sun, S.; Wucher, A.; Winograd, N. *Appl. Surf. Sci.* **2004**, *231*−*231*, 183.
(40) Mahoney, C. M.; Yu, J.; Gardella, J. A. *Anal. Chem.* **2005**, *77*, 3570.
(41) Wagner, M. S. *Anal. Chem.* **2004**, *76*, 1264.
(42) Deline, V. R.; Evans, C. A.; Williams, P. *Appl. Phys. Lett.* **1978**, *33*, 578.
(43) Storms, H. A.; Brown, K. F.; Stein, J. D. *Anal. Chem.* **1977**, *49*, 2023.
(44) Williams, P.; Lewis, R. K.; Evans, C. A.; Hanley, P. R. *Anal. Chem.* **1977**, *49*, 1399.
(45) Franzreb, K.; Lorincik, J.; Williams, P. *Surf. Sci.* **2004**, *573*, 291.
(46) Krohn, V. E. *J. Appl. Phys.* **1962**, *33*, 3523.
(47) Matyjaszewski, K.; Xia, J. *Chem. Rev.* **2001**, *101*, 2921.
(48) Xia, J.; Matyjaszewski, K. *Macromolecules* **1997**, *30*, 7697.
(49) Matyjaszewski, K.; Patten, T. E.; Xia, J. H. *J. Am. Chem. Soc.* **1997**, *119*, 674.

Table 1. Characteristics of Polymer Utilized: Polymer Molecular Weights and Polydispersities As Measured Using GPC (30 °C, $CHCl_3$), and T_g's Measured Using DSC (10 °C/min Cooling Cycle)

polymer	M_w/kDa	M_w/M_n	T_g/°C
^{13}C-PS	79.4	1.20	100
^{12}C-PS	73.7	1.19	100
PMMA	90.9	1.26	100

Table 2. Polymer/Solvent Solutions Used To Prepare the Six Different Sample Types[a]

solution	mass polymer	% ^{13}C-PS (v/v)	vol (mL)/solvent
1	40 mg ^{13}C-PS	100	1/toluene
2	90 mg ^{12}C-PS	0	3/toluene
3	6 mg ^{13}C-PS + 111 mg ^{12}C-PS	5	3/1-chloropentane
4	115 mg PMMA	0	3/toluene
5	15 mg ^{13}C-PS	100	2/benzene
6	15 mg ^{12}C-PS	0	2/benzene

[a] Volume percent ^{13}C-PS is on a solvent-free basis (i.e., concentration in the cast film).

for 30 min. The flask was then immersed in an oil bath held at 90 °C, its content continuously stirred using a magnetic stir bar, and 42 μL of ethyl 2-bromoisobutyrate (98%, Sigma-Aldrich) was injected. The reaction was stopped after 4 h, and the solution was diluted with THF and run through an activated neutral alumina column. The solution was then precipitated into 2 L of hexanes (Fisher), filtered, and dried overnight at 70 °C. Using DSC, the T_g was determined to be 100 °C (10 °C/min cooling cycle), implying a somewhat random monomeric sequence distribution (atactic PMMA).[50] This was further confirmed using proton nuclear magnetic resonance spectroscopy[51,52] (^{1}H NMR, Varian Mercury 400 MHz) in deuterium-labeled chloroform (99.8%, Aldrich), which shows 4% isotactic, 38% heterotactic, and 58% syndiotactic triad distributions (*mm*, *mr*, and *rr*, respectively). PMMA tacticity is highly sensitive to the choice of polymerization technique (i.e., radical or anionic) and conditions (i.e., temperature, solvent, and initiator).[52] The molecular weight and polydispersity were measured using GPC with a $CHCl_3$ diluent at 30 °C, after calibration with atactic PS standards, and converted to the correct values for atactic PMMA using the universal calibration principle[53] with known Mark−Houwink parameters for atactic PS ($K = 4.9 \times 10^{-3}$ mL/g; $a = 0.794$) and atactic PMMA ($K = 4.3 \times 10^{-3}$ mL/g; $a = 0.80$).[54] The characteristics of the polymers utilized are summarized in Table 1.

Sample Preparation. Six solutions (summarized in Table 2) were prepared for six different sample types. First, HPLC grade benzene (Aldrich) was distilled over calcium hydride and stored under N_2. Toluene (Fisher), 1-chloropentane (Sigma-Aldrich), and HPLC grade *n*-heptane (Aldrich) were used as received. Silicon (100) wafers were cut to 2.5 cm × 2.5 cm squares, soaked in BakerClean JTB-111 (J.T. Baker) for 30 min, and subsequently washed with deionized (DI) water. They were then etched in 10% (v/v) aqueous hydrofluoric acid, washed with DI water, and placed in a UV−ozone oven for 30 min to build a SiO_x layer (~2 nm) on the hydrogen-passivated Si surface. Samples prepared for dynamic SIMS (depth profiling) were all spin-cast at 3000 rpm (samples A−D). For samples C and D, solution 4 was cast and annealed for 30 min at 125 °C. Solution 3 was then cast directly onto the PMMA layer, as 1-chloropentane is a selective solvent for PS over PMMA. For samples A−C, the bottom layer(s) were annealed at 125 °C for 24 h, and then the top ^{12}C-PS layer was cast onto the Si + SiO_x substrates, scored with a sharp tip, floated into DI water, and picked up with the bottom layer(s). These polymer film assemblies were then annealed at 80 °C for 12 h to remove residual solvent while preventing interdiffusion.[55] For sample D, the bottom layers were annealed at 125 °C for 24 h, and the top PMMA layer was cast onto a microscope cover glass, scored with a sharp tip, floated into water, and picked up with the bottom layers. This polymer film assembly was annealed at 125 °C for 3 h. Samples for TOF SIMS analysis (samples E and F) were prepared using a procedure that was outlined previously.[56] ^{13}C-PS (solution 5) and ^{12}C-PS (solution 6) were spin-cast at 5000 rpm onto individual substrates and annealed on a hot plate, which had been cleaned with *n*-heptane, for 5 min at 100 °C to remove residual solvent. The samples were then washed with *n*-heptane to remove any potential surface contaminants, such as poly(dimethylsiloxane). All layer thicknesses were measured individually using single-wavelength ellipsometry (Rudolph Auto El III). Properties of all six sample types (samples A−F) are summarized in Table 3.

Table 3. Six Different Sample Types Utilized[a]

sample	soln$_1$	h_1 (nm)	method$_1$	soln$_2$	h_2 (nm)	method$_2$	soln$_3$	h_3 (nm)	method$_3$
A	1	180	C	2	125	F		0	
B	3	175	C	2	125	F		0	
C	4	145	C	3	175	C	2	125	F
D	4	145	C	3	175	C	4	145	F
E	5	70	C		0			0	
F	6	70	C		0			0	

[a] Showing the solutions from Table 2 used for each corresponding layer ($n = 1$, 2, or 3), the thickness of the layer (h_n) as measured using ellipsometry, and the method used to prepare the corresponding layer (i.e., direct casting C or floating F).

Secondary Ion Mass Spectrometry. All depth profiles were performed using a Cameca IMS-6f magnetic sector mass spectrometer. A 20-nm (nominal) Au coating was sputtered onto samples A−D before the SIMS analysis to help minimize charging. Even though the Au in the rastered area is removed at the beginning of the analysis, the remaining Au surrounding the raster crater provides a conductive path for charge removal (passive charge neutralization).[32,57] Typical analysis conditions for O_2^+

(50) Fuchs, K.; Friedrich, C.; Weese, J. *Macromolecules* **1996**, *29*, 5893.
(51) Frisch, H. L.; Mallows, C. L.; Bovey, F. A. *J. Chem. Phys.* **1966**, *45*, 1565.
(52) Ferguson, R. C. *Macromolecules* **1969**, *2*, 237.
(53) Dobkowski, Z. *J. Appl. Polym. Sci.* **1984**, *29*, 2683.
(54) Brandrup, J., Immergut, E. H., Grulke, E. A., Eds. *Polymer Handbook,* 4th ed.; Wiley-Interscience: Hoboken, NJ, 1999; Vol. 2.
(55) Agrawal, G.; Wool, R. P.; Dozier, W. D.; Felcher, G. P.; Zhou, J.; Pispas, S.; Mays, J. W.; Russell, T. P. *J. Polym. Sci., Part B: Polym. Phys.* **1996**, *34*, 2919.
(56) Vanden Eynde, X.; Bertrand, P.; Penelle, J. *Macromolecules* **2000**, *33*, 5624.
(57) McKinley, J. M.; Stevie, F. A.; Granger, C. N.; Renard, D. *J. Vac. Sci. Technol., A* **2000**, *18*, 273.

Table 4. Sputtering Rates S_R, Approximated Using the Known Thicknesses of the Various Layers in Samples A−D and the Known Sputtering Times and Raster Areas[a]

	O_2^+ S_R (nm^3/ion)	O_2^+ $S_R/S_{R,Si}$	Cs^+ S_R (nm^3/ion)	Cs^+ $S_R/S_{R,Si}$
Si (100)	0.033	1.0	0.095	1.0
PS	0.046	1.1	0.11	1.4
PMMA	0.11	3.2	0.30	3.4

[a] Values are also normalized using measured values for intrinsic Si (100) ($S_R/S_{R,Si}$).

primary ion bombardment included a 30-nA primary current rastered over a 180 μm × 180 μm area, with 5.5-keV impact energy (10 kV primary with 4.5 kV sample bias) and $m/\Delta m = 3000$. The angle of incidence for the primary ions was 41°. Transport of ions in matter (TRIM) simulations,[58] using the SRIM-2003 commercial software package, show a penetration depth $R_p \approx 10$ nm with a straggle $\Delta R_p \approx 5$ nm for O_2^+ implantation into PS and PMMA under these conditions. Positive secondary ions were detected from a 60-μm-diameter optically gated area positioned in the center of the raster. For Cs^+, typical analysis conditions included a 10-nA primary current rastered over a 180 μm × 180 μm area, with 6.0-keV impact energy (5 kV primary with −1 kV sample bias) and $m/\Delta m = 2910$. The angle of incidence for the primary ions was 27°. TRIM simulations show $R_p \approx 17$ nm with $\Delta R_p \approx 3$ nm for Cs^+ implantation into PS and PMMA under these conditions. Negative secondary ions were detected from a 60-μm-diameter optically gated area positioned in the center of the raster. For sample C, charge neutralization for Cs^+ bombardment with detection of negative secondary ions was evaluated using the so-called "electron cloud" method.[33] Electrons at normal incidence to the sample are provided with a potential just below that of the sample and are present just above the surface. In this self-compensating method, any charging due to ion bombardment of the surface of the sample is compensated by electrons that are drawn from the electron cloud. For 5-kV primary ions with a −1-kV sample bias, the typical electron coverage area is ~125 μm in diameter and an ion beam raster 110 μm × 110 μm (30-μm diameter detection area) was used for the analysis. At least two spots per sample were analyzed for samples A−D. TOF SIMS analyses (static SIMS) were performed using a PHI TRIFT I TOF mass spectrometer with 15-keV Ga^+ primary ion energy and detection of positive secondary ions. A 600-pA primary ion current was used over a 100 μm × 100 μm detection area with a 7.2-kV extraction voltage. Data acquisition time was set to 7 min, resulting in a total ion fluence of ~5 × 10^{11} ions/cm^2 per analysis. Mass spectra collected for three different spots for samples E and F were analyzed using WinCadence software.

RESULTS AND DISCUSSION

The sputtering rates S_R for PS and PMMA were determined for both 5.5-keV O_2^+ and 6.0-keV Cs^+ bombardment from the known thicknesses of the various layers for systems A−C as determined using ellipsometry. The rate approximations are summarized in Table 4. The real space depth profiles of sample A, using the typical analysis conditions for Cs^+ and O_2^+ primary ion bombardment as described above, are shown in Figure 3. In Figure 3a and b, the $^{12}C^1H$ profile clearly traces the ^{12}C profile but not that of ^{13}C. This clearly establishes that $^{12}C^1H$ and ^{13}C have been completely mass resolved. High ^{13}C detection sensitivity for Cs^+ and O_2^+ bombardment is also revealed via the efficient detection of the ^{13}C background (natural abundance) in the top ^{12}C-PS layer. Panels c and d of Figure 3 show the normalized profiles for the experimental volume fraction of ^{13}C-PS (φ) as a function of effective depth (z), based on the PS sputtering rates, as determined by

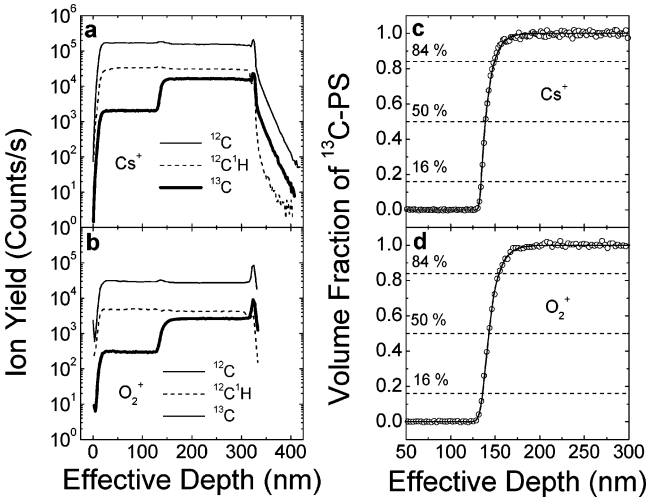

Figure 3. SIMS depth profiles of sample A (a, b) showing ^{12}C (solid line), $^{12}C^1H$ (dashed line), and ^{13}C (bold line) secondary ion yields and (c, d) volume fraction of ^{13}C-PS in the ^{12}C-PS/^{13}C-PS bilayer. Both (a, c) 6.0-keV Cs^+ and (b, c) 5.5-keV O_2^+ primary ion bombardment, with detection of negative and positive secondary ions, respectively, provide high S/N and high detection sensitivity. $^{12}C^1H$ is completely mass resolved from ^{13}C for both primary ions. Shown in (c) and (d) are the midpoint (50%) and 16 and 84% intensity lines, which are used to semiquantitatively describe the asymmetry of the profiles (see Table 5). The solid lines in (c) and (d) are a fit using a step function convoluted with a Gaussian and an exponential function (see eqs 2−4), resulting in the regression parameters summarized in Table 5. (The effective depth was determined by assuming a constant PS sputtering rate throughout the film assembly.).

$$\varphi(z) = \frac{Y_{13}(z) - Y_{NA}}{Y_P - Y_{NA}} \quad (1)$$

where $Y_{13}(z)$ is the ^{13}C ion yield, normalized to the total atomic C (^{12}C + ^{13}C) ion yield, at depth z, Y_{NA} is the normalized ^{13}C ion yield of pure ^{12}C-PS (natural abundance), and Y_P is the normalized ^{13}C ion yield of pure ^{13}C-PS. Under the conditions implemented here for both O_2^+ and Cs^+ bombardment, excellent signal-to-noise ratio (S/N) is observed in the profiles in Figure 3c and d, even though there is only 10.3% ^{13}C in the ^{13}C-PS (relative to ^{12}C + ^{13}C), as determined using TOF SIMS (see below).

The experimental profiles shown in Figure 3c and d for 6.0-keV Cs^+ and 5.5-keV O_2^+ reveal asymmetric profiles through the ^{12}C-PS/^{13}C-PS interface for both ion probes. The experimental widths corresponding to 84/16 ($(2\sigma)_{84/16}$), 50/16 ($\sigma_{50/16}$), and

(58) Ziegler, J. F.; Biersack, J. P.; Littmark, U. *The Stopping and Range of Ions in Solids*; Pergamon: New York, 1985.

Table 5. Widths of the Profiles Shown in Figure 1c,d Based on 84/16 ($(2\sigma)_{84/16}$), 50/16 ($\sigma_{50/16}$), and 84/50 ($\sigma_{84/50}$) Intensity Crossings, and Regressed Parameters σ_{eff} and λ_d (Eqs 2−4)

	$(2\sigma)_{84/16}$ (nm)	$\sigma_{50/16}$ (nm)	$\sigma_{84/50}$ (nm)	σ_{eff} (nm)	λ_d (nm)
O_2^+	19	7	12	4.2	10
Cs^+	14	5	9	1.7	9

84/50 ($\sigma_{84/50}$) intensity changes are tabulated in Table 5. The differences between the $\sigma_{50/16}$ and $\sigma_{84/50}$ values are a measure of the asymmetry. Furthermore, the 84/16 depth resolution for 6.0-keV Cs^+ is better than that with 5.5-keV O_2^+ primary ion bombardment ($(2\sigma)_{84/16} = 14$ and 19 nm, respectively), which is consistent with previous observations.[44,59]

The profile line shapes and nearly a factor of 2 difference between $\sigma_{50/16}$ and $\sigma_{84/50}$ observed through the ^{12}C-PS/^{13}C-PS interface clearly demonstrate that these profiles cannot be accurately represented by a symmetric Gaussian instrument resolution convoluted with a sharp intrinsic profile. The observed convolution type arises primarily from ion-induced mixing of the ^{13}C and ^{12}C matrix and implantation of the ^{13}C further into the film (tailing).[60] Analogous behavior has been observed for ^{30}Si implants in a ^{28}Si matrix.[60] A physically meaningful convolution function is required in order to compare SIMS depth profiles to various theoretical models when probing physical phenomena at polymer surfaces and heterogeneous interfaces.[16,21] Here we employ a simplified version of a convolution scheme that has been outlined previously.[60,61] It combines a Gaussian with a standard deviation σ_{eff} that accounts for ion-induced mixing and sources of uncorrelated convolution, such as sample roughness and intrinsic interfacial width,[16,17] and an exponential for the observed tailing, which has a characteristic decay length λ_d. The Gaussian convolution function is

$$G(z) = \frac{1}{(2\pi)^{1/2}\sigma_{eff}} \exp\left[-\frac{1}{2}\left(\frac{z}{\sigma_{eff}}\right)^2\right]; \quad z \rightarrow (-\infty,\infty) \qquad (2)$$

and the exponential decay is described by

$$F(z) = \frac{1}{\lambda_d} \exp\left(-\frac{z}{\lambda_d}\right); \quad z \rightarrow (0,\infty) \qquad (3)$$

$G(z)$ and $F(z)$ are numerically convoluted, using the Fourier transform method,[62] with a Heaviside step function $\theta(z)$,[16] where

$$\theta(z) = 0 \ (-\infty, z_I) \quad \text{and} \quad \theta(z) = 1 \ (z_I, \infty) \qquad (4)$$

to approximate the experimental profiles. These convoluted profiles are fit to the data with σ_{eff} and λ_d as regression parameters.

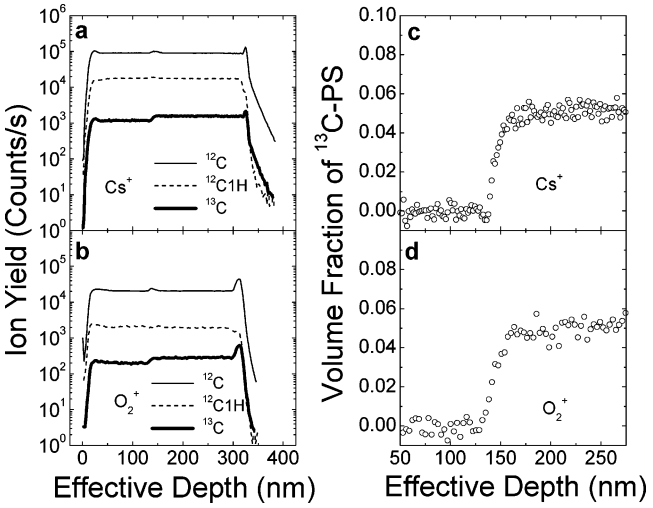

Figure 4. SIMS depth profiles of sample B, a bilayer consisting of ^{12}C-PS (top) and 5% (v/v) ^{13}C-PS + ^{12}C-PS, showing (a, b) ^{12}C (solid line), ^{12}C^{1}H (dashed line), and ^{13}C (bold line) secondary ion yields and (c, d) volume fraction of ^{13}C-PS as a function of effective depth. The use of (a, c) 6.0-keV (10 nA) Cs^+ primary ion bombardment provides greatly improved detection sensitivity and S/N for depth profiling of ^{13}C-PS when compared to (b, d) 5.5-keV (30 nA) O_2^+ bombardment.

Results for 6.0-keV Cs^+ and 5.5-keV O_2^+ primary ion bombardment are summarized in Table 5. The best fit line shapes are also plotted as solid lines in the graphs shown in Figure 3c and d, clearly indicating that the combination of a Gaussian and exponential decay function yields excellent results. The effective location of the interface z_I was determined by the fit. Although an attempt has been made to put physical meaning into the functionalization of the profiles shown in Figure 3c and d, molecular-level complexities inherent to SIMS analysis of polymer films[25,63] make further interpretation of the regressed parameters Δ_{eff} and λ_d difficult.

The detection sensitivity and S/N were further evaluated using sample B, which contains a layer of 5% (v/v) ^{13}C-PS + ^{12}C-PS and a top layer of 100% ^{12}C-PS. Here, the ^{13}C-PS doped film only contains ~40% ^{13}C above the natural-abundance background. Figure 4 shows the depth profiles analyzed using both 6.0-keV Cs^+ and 5.5-keV O_2^+ primary ion bombardment. Panels a and b of Figure 4 show complete mass resolution of ^{12}C^{1}H from ^{13}C and a marginal increase in ^{13}C secondary ion yield from the ^{12}C-PS top layer to the ^{13}C-PS doped layer. The normalized profiles in Figure 4c and d show decreased S/N compared to the profiles in Figure 3c and d. Furthermore, 6.0-keV (10 nA) Cs^+ provides higher detection sensitivity and S/N than 5.5-keV (30 nA) O_2^+ for ^{12}C, ^{13}C, and ^{12}C^{1}H. It is well known that Cs^+ primary ion bombardment often provides improved detection sensitivity, depth resolution, and sputtering efficiency (see Table 4), all of which are observed here, for a variety of detected species and matrixes when compared to O_2^+ under similar conditions.[25,44] Unfortunately, the use of Cs^+ has also been observed to produce somewhat anomalous secondary ion yields through a heterogeneous polymer/polymer interface, particularly with the PS/PMMA interface.[10] As shown in Figure 5 (sample C), there is quite a difference in secondary ion yields through the ^{13}C-PS:^{12}C-PS/PMMA interface for 6.0-keV Cs^+ (Figure 5a) that is absent for 5.5-keV O_2^+ (Figure 5b) primary ion bombardment.

(59) Harton, S. E.; Koga, T.; Stevie, F. A.; Araki, T.; Ade, H. *Macromolecules* **2005**, *38*, 10511.
(60) Dowsett, M. G.; Barlow, R. D.; Allen, P. N. *J. Vac. Sci. Technol., B* **1994**, *12*, 186.
(61) Allen, P. N.; Dowsett, M. G. *Surf. Interface Anal.* **1994**, *21*, 206.
(62) Press: W. H.; Flannery, B. P.; Teukolsky, S. A.; Vetterling, W. T. *Numerical Recipes in Fortran 77: The Art of Scientific Computing,* 2nd ed.; Cambridge University Press: New York, 1992.
(63) Delcorte, A.; Bertrand, P.; Garrison, B. J. *J. Phys. Chem. B* **2001**, *105*, 9474.

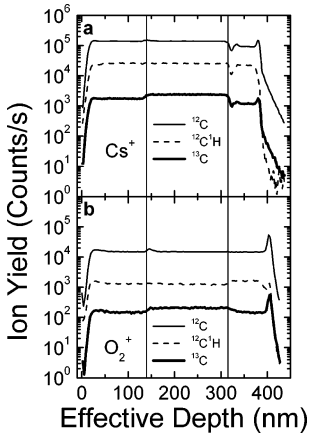

Figure 5. SIMS depth profiles of sample C using (a) 6.0-keV (10 nA) Cs^+ and (b) 5.5-keV (30 nA) O_2^+ primary ion bombardment. The effective depth was determined by assuming a constant PS sputtering rate throughout the film assembly. The two vertical lines show the approximate location of both the ^{12}C-PS/^{12}C-PS:^{13}C-PS (~135 nm) and ^{12}C-PS:^{13}C-PS/PMMA (~310 nm) interfaces.

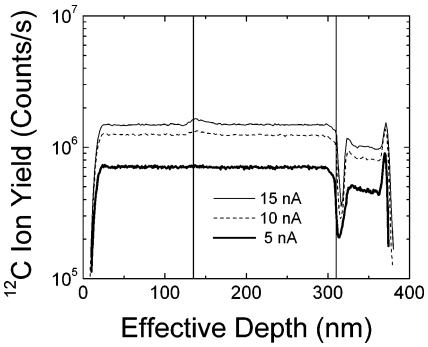

Figure 6. Effect of variation of 6.0-keV Cs^+ primary ion current on SIMS depth profile of sample C. The nonmonotonic changes in the secondary ion yields at the ^{12}C-PS:^{13}C-PS/PMMA interface (~310 nm) appear to be nearly independent of primary ion current. This supports the conclusion that sample charging is not the underlying cause of the behavior observed at the heterogeneous polymer/polymer interface. The two vertical lines show the approximate location of both the ^{12}C-PS/^{12}C-PS:^{13}C-PS (~135 nm) and ^{12}C-PS:^{13}C-PS/PMMA (~310 nm) interfaces. (The effective depth was determined by assuming a constant PS sputtering rate throughout the film assembly.).

Even though the anomalous ^{12}C secondary ion yield at the ^{13}C-PS/^{12}C-PS/PMMA interface is nearly independent of Cs^+ primary ion current (Figure 6), implying that sample charging is not the underlying cause of these nonmonotonic changes in secondary ion yields through the interface, sample charging was explicitly ruled out by evaluating ^{12}C secondary ion energy spectra at various locations through the film and through the use of active charge neutralization with the so-called electron cloud method.[33] These energy spectra of a 3-nA Cs^+ primary ion beam rastered over a 110 μm × 110 μm area are shown in Figure 7 along with the approximate depth at which each spectrum was recorded (inset). No significant shift in the location of the ^{12}C yield maximum is observed, and a shift would be expected if sample charging occurred. Using Cs^+ primary beam and charge neutralization with the electron cloud method, depth profiles were generated and are shown in Figure 8. Again, similar to Figures 5 and 6, the secondary ion yield through the PS/PMMA interface was nonmonotonic, even though the sample has now been adequately charge

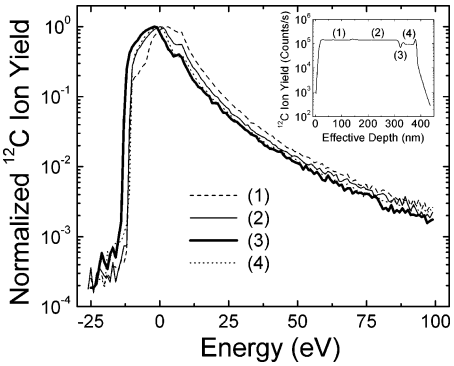

Figure 7. ^{12}C Secondary ion energy spectra at various depths (inset) for sample C using 6.0-keV (3 nA) Cs^+ primary ion bombardment. No signs of charging are present at any depth in the sample.

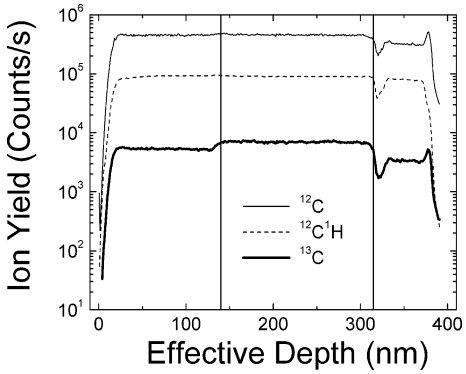

Figure 8. SIMS depth profile analysis of sample C using 6.0-keV Cs^+ ion bombardment (3 nA, 110 μm × 110 μm raster) and the electron cloud method of charge neutralization. The two vertical lines show the approximate location of both the ^{12}C-PS/^{12}C-PS:^{13}C-PS (~135 nm) and ^{12}C-PS:^{13}C-PS/PMMA (~310 nm) interfaces. The nonmonotonic changes in the secondary ion yields at the ^{12}C-PS:^{13}C-PS/PMMA interface are still apparent, again proving that sample charging is not the underlying cause of this behavior. This also confirms that the electron cloud method of charge neutralization can be implemented without causing excess damage to the polymer film. (The effective depth was determined by assuming a constant PS sputtering rate throughout the film assembly.)

compensated. This is significant for two very important reasons. First, the anomalous behavior observed with the secondary ion yields at the PS/PMMA interface (see Figure 5a) is clearly not due to sample charging. Second, this confirms that the electron cloud method of charge neutralization, which is only currently used on a magnetic sector SIMS instrument,[33] can be implemented during analysis of systems involving organic species without causing sample degradation because the electrons do not impact the sample, thereby permitting these types of analyses to include a broad range of polymer systems and sample thicknesses.

In an attempt to gain insight into the underlying mechanism behind the changes in secondary ion yields at the PS/PMMA interface, a trilayer consisting of PMMA as the top and bottom layers, with 5% (v/v) ^{13}C-PS + ^{12}C-PS in the middle layer (sample D), was assembled to look at the interface while sputtering through an interface from PMMA to PS and PS to PMMA, respectively. SIMS analysis was performed with a 3-nA (6.0-keV) Cs^+ primary ion bombardment rastered over a 180 μm × 180 μm area. Figure 9 clearly shows somewhat erratic changes in secondary ion yields through both interfaces, although the behavior is quite different at each interface, almost the inverse of

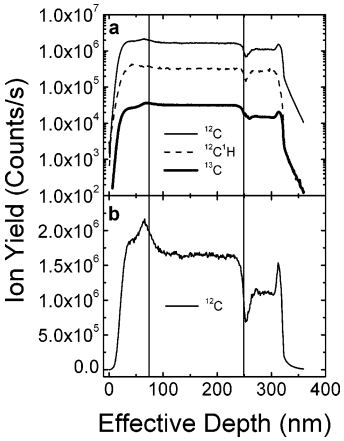

Figure 9. Characterization of a PMMA/^{12}C-PS:^{13}C-PS/PMMA film (sample D) using 6.0-keV (10 nA) Cs^+ primary ion bombardment. The effective depth was determined by assuming a constant PS sputtering rate throughout the film assembly. The two vertical lines show the approximate location of both the PMMA/^{12}C-PS:^{13}C-PS (~75 nm) and ^{12}C-PS:^{13}C-PS/PMMA (~250 nm) interfaces. Changes in ^{12}C, ^{12}C^{1}H, and ^{13}C secondary ion yields are apparent through both interfaces (a), although the behavior is quite different at each interface. A plot of the ^{12}C secondary ion yield on a linear scale has also been provided (b) in order to highlight the changes in secondary ion yields at both PS/PMMA interfaces.

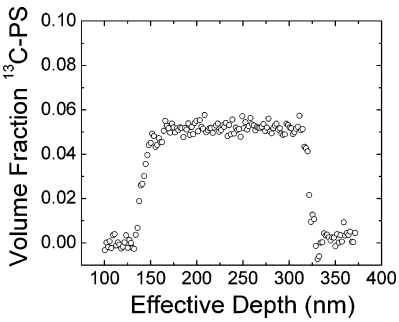

Figure 10. ^{13}C-PS SIMS depth profile for Sample C, showing that normalization of the ^{13}C ion yield to the total C ($^{12}C + {}^{13}C$) ion yield (see eq 1) can help to alleviate the nonmonotonic behavior at the heterogeneous ^{12}C-PS:^{13}C-PS/PMMA interface. The ^{12}C-PS/^{12}C-PS:^{13}C-PS and ^{12}C-PS:^{13}C-PS/PMMA interfaces are located at ~135 and 310 nm, respectively.

each other. A plot on a linear scale has also been provided in Figure 9b in order to highlight the changes in secondary ion yields at both PS/PMMA interfaces. A possible mechanism may be a loss of constant equilibrium primary ion concentration (transient sputtering) when sputtering through the heterogeneous PS/PMMA interfaces, which could be caused by the large difference in sputtering rates between PS and PMMA (see Table 4). Some difference in sputtering rate and secondary ion yield typically occurs at the onset of dynamic SIMS analysis because the amount of the analysis beam present varies until the implant range of the anlysis beam has been reached,[23] necessitating the addition of a sacrificial layer to the film or multilayer before the analysis, which is composed of a polymer identical to the top layer, if accurate profiling of the surface region is required.[9,10]

Further investigation into yield changes across interfaces will be necessary for a better understanding of this intriguing system. Fortunately, the method delineated here that relies on ^{13}C labeling might greatly help to alleviate nonmonotonic yield changes as ^{13}C

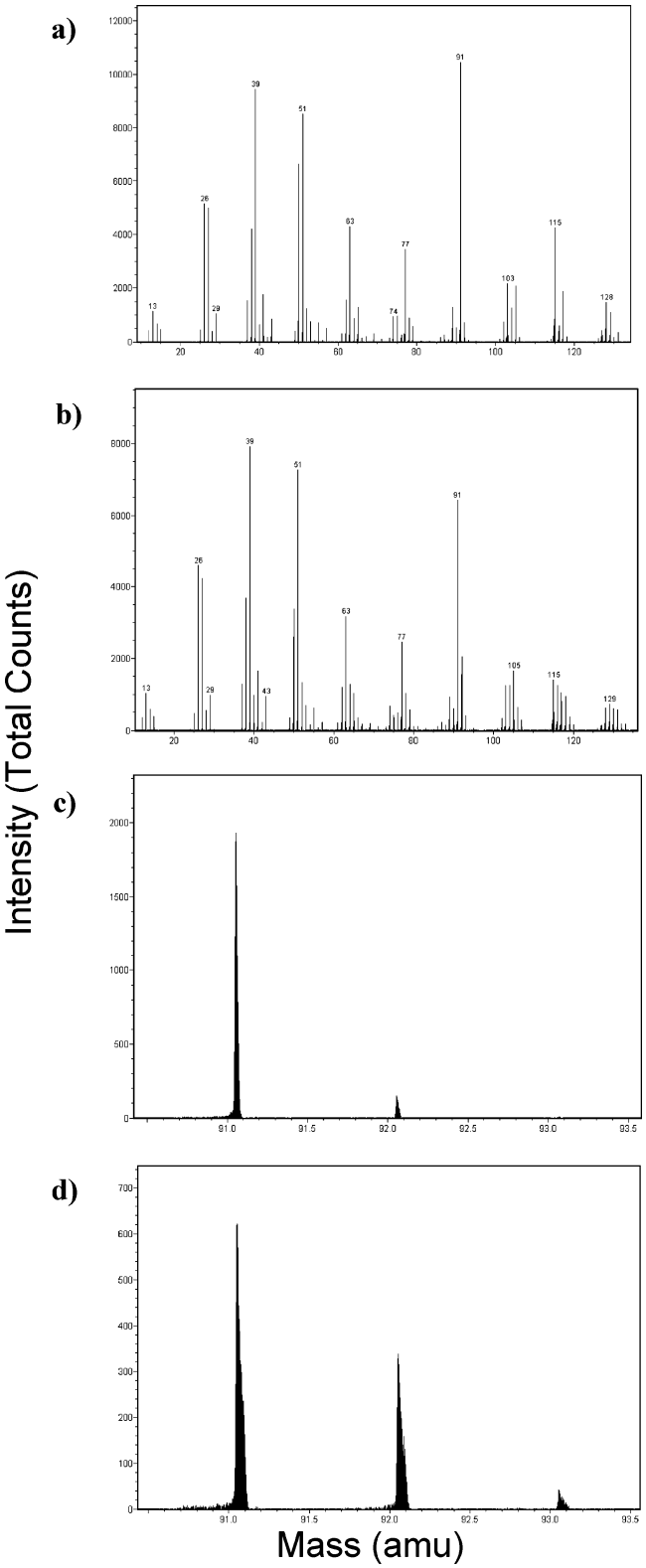

Figure 11. TOF SIMS (15 keV Ga^+) positive secondary ion mass spectra (total counts) for (a) ^{12}C-PS (sample E) and (b) ^{13}C-PS (sample F) from approximately 10 to 130 amu (0.15 amu bin) and (c) ^{12}C-PS and (d) ^{13}C-PS from approximately 91 to 93 amu (0.004 amu bin). Natural abundance of ^{13}C in ^{12}C-PS was verified with (c), demonstrating that there are negligible mass interferences for the C_7H_7 fragment.

secondary ion yields should be affected nearly identically to ^{12}C matrix ion yields through heterogeneous interfaces. Through

normalization of the ^{13}C secondary ion yield to the total C ($^{12}C + {}^{13}C$) ion yield (see eq 1), changes such as those that occur through the PS/PMMA interface can be greatly minimized. The ^{13}C SIMS depth profile from Figure 5a has been normalized in this manner and is shown in Figure 10. There is no readily observable artifact or segregation of ^{13}C-PS to the ^{13}C-PS:^{12}C-PS/PMMA interface. In contrast, prior results using an analogous ^{1}H-PS:^{2}H-PS/PMMA system have shown strong segregation of 83-kDa ^{2}H-PS (^{13}C-PS used here is 79.4 kDa) to the heterogeneous interface at 138 °C[21] (Note: there is less than a 15% change in the ^{1}H-PS:^{2}H-PS phase diagram shown in Figure 1 from 125 to 138 °C[20]). Therefore, the use of ^{13}C labeling can greatly improve the characterization of polymer films and multilayers using SIMS and improve the physical and theoretical interpretation of various experimentally observed phenomena at polymer/polymer heterogeneous interfaces, such as reactive coupling[11,12] and polymer chain mobility,[13,14] because the effects of tracer labeling on the properties of the system are greatly reduced.

Finally, with the recent advances in the use of high molecular weight cluster probes for TOF SIMS analysis,[27,34] depth profiling of high molecular weight fragments (~100 amu) has become possible.[37−40] This may lead to future use of TOF SIMS for high-resolution depth profiling of ^{13}C-labeled polymers. To evaluate this possibility, we have looked at the mass spectra of ^{13}C-PS and ^{12}C-PS (samples E and F, respectively) using a PHI TRIFT I TOF mass spectrometer with 15-keV Ga^+ primary ion bombardment and detection of positive secondary ions, as shown in Figure 11. Subtle differences can be found between the spectra of ^{12}C-PS (Figure 11a) and ^{13}C-PS (Figure 11b), but particular attention is paid to the intense tropylium ion peak at 91.05474 amu ($^{12}C_7{}^{1}H_7^+$)[64] and its isotopically labeled analogues (Figure 11c and d). From Figure 11c, natural abundance of ^{13}C is determined from the peaks at 91 and 92 amu (nominal) for ^{12}C-PS, thereby demonstrating that there are no significant mass interferences for this fragment. Quantitative depth profiling of high molecular weight fragments, such as the intense tropylium fragment in PS,[64] may be possible under highly optimized conditions,[37,39] requiring low primary ion implant depths and efficient removal of damaged molecular layers.[30]

CONCLUSIONS

The use of ^{13}C labeling as an alternative to deuterium labeling for depth profiling of polymer films and multilayers using SIMS has been introduced. By minimizing the changes in bulk[19,20] and surface properties[2,15] of polymers and polymer blends due to isotopic labeling, significant improvements can now be obtained when probing various physical phenomena at polymer surfaces and heterogeneous interfaces.[21] To mass resolve $^{12}C^{1}H$ (13.007 82 amu) from ^{13}C (13.003 35 amu), which requires $m/\Delta m \approx 3000$, a magnetic sector mass spectrometer (Cameca IMS-6f) was used with both 6.0-keV impact energy Cs^+ and 5.5-keV impact energy O_2^+ primary ions, with detection of negative and positive secondary ions, respectively. Complete mass resolution of $^{12}C^{1}H$ from ^{13}C was achieved for 6.0-keV Cs^+ and 5.5-keV O_2^+ primary ion bombardment in a ^{12}C-PS/^{13}C-PS bilayer film. This type of analysis cannot be performed with a quadrupole mass spectrometer, with a typical $m/\Delta m \sim 300$.[31] It was shown that the convolution of the depth profiles analyzed here have to be described by a combination of a Gaussian and an exponential function. The parameters derived from a fit to this combined convolution function have been summarized in Table 5 for both 6.0-keV Cs^+ and 5.5-keV O_2^+, thereby permitting future analyses to involve comparison of the SIMS profiles to various theoretical models.[16,21] It has also been shown that 6.0-keV Cs^+ provides improved detection sensitivity and S/N over 5.5-keV O_2^+ primary ion bombardment when depth profiling ^{13}C-labeled polymers, although analysis using Cs^+ appears to be much more susceptible to changes in secondary ion yields through a heterogeneous polymer/polymer interface such as the PS/PMMA interface.[10] Sample charging was conclusively ruled out as the underlying cause of this behavior at the PS/PMMA interface. By using ^{13}C as a tracer, these matrix effects could be greatly reduced when depth profiling ^{12}C-PS:^{13}C-PS/PMMA multilayers, thereby proving that the use of this novel technique provides a true tracer for analysis of polymer systems. Finally, mass spectra of ^{13}C-PS and ^{12}C-PS were analyzed using TOF SIMS (15-keV Ga^+ with detection of positive secondary ions) with a PHI TRIFT I mass spectrometer to evaluate the potential use of TOF SIMS for depth profiling of relatively high molecular weight fragments (~100 amu) of ^{13}C-labeled polymers. Detection of $C_7H_7^+$ secondary ions, having significant detection sensitivities and negligible mass interferences, was proposed for future investigations into quantitative molecular depth profiling using TOF SIMS.

ACKNOWLEDGMENT

This work was supported by the U.S. Department of Energy (DE-FG02-98ER45737). The authors gratefully acknowledge discussions with Prof. Bruce Novak regarding the polymer synthesis and Dr. Dieter Griffis regarding the SIMS analysis. We also thank Prof. Alan Tonelli for providing helpful comments on the manuscript.

Received for review January 18, 2006. Accepted March 9, 2006.

AC060133O

(64) Affrossman, S.; Hartshorne, M.; Jerome, R.; Munro, H.; Pethrick, R. A.; Petitjean, S.; Vilar, M. R. *Macromolecules* **1993**, *26*, 5400.